Analyst

ROYAL SOCIETY OF CHEMISTRY

PAPER

View Article Online
View Journal | View Issue

Check for updates

Cite this: *Analyst*, 2023, **148**, 1514

Mobile multi-configuration clinical translational Raman system for oral cancer application

Siddra Maryam, *[a] Sanathana Konugolu Venkata Sekar,[a] M. Daniyal Ghauri,[a] Edward Fahy,[b] Marcelo Saito Nogueira,[a] Huihui Lu,[a] Flavien Beffara,[c] Georges Humbert,[c] Richeal Ni Riordain,[b,d] Patrick Sheahan,[e] Ray Burke,[a] Kiang Wei Kho,[a] Rekha Gautam [a] and Stefan Andersson-Engels [a]

Early diagnosis of oral cancer is critical to improve the survival rate of patients. Raman spectroscopy, a non-invasive spectroscopic technique, has shown potential in identifying early-stage oral cancer biomarkers in the oral cavity environment. However, inherently weak signals necessitate highly sensitive detectors, which restricts widespread usage due to high setup costs. In this research, the fabrication and assembly of a customised Raman system that can adapt three different configurations for the *in vivo* and *ex vivo* analysis is reported. This novel design will help in reducing the cost required to have multiple Raman instruments specific for a given application. First, we demonstrated the capability of a customized microscope for acquiring Raman signals from a single cell with high signal-to-noise ratio. Generally, when working with liquid samples with low concentration of analytes (such as saliva) under a microscope, excitation light interacts with a small sample volume, which may not be representative of whole sample. To address this issue, we have designed a novel long-path transmission set-up, which was found to be sensitive towards low concentration of analytes in aqueous solution. We further demonstrated that the same Raman system can be incorporated with the multimodal fibre optical probe to collect *in vivo* data from oral tissues. In summary, this flexible, portable, multi-configuration Raman system has the potential to provide a cost-effective solution for complete screening of precancer oral lesions.

Received 23rd November 2022,
Accepted 22nd February 2023

DOI: 10.1039/d2an01921c

rsc.li/analyst

Open Access Article. Published on 06 March 2023. Downloaded on 7/20/2024 1:21:36 AM.
This article is licensed under a Creative Commons Attribution-NonCommercial 3.0 Unported Licence.

1. Introduction

Oral cancer refers to pathologies affecting the tongue, floor of mouth, upper and lower alveolus, palate, and buccal mucosa.[1,2] It is described as 16th most common cancer worldwide, often detected in advanced stage, resulting in an overall survival rate of 40–60%.[3] The survival rate could be significantly improved to <80% [4–6] if detected in precancerous stage. Primary care delays in recognizing suspicious symptoms remains an ongoing problem in cancer diagnosis.[7] To address this, previously various physician-friendly point-of-care optical techniques that can provide easy, inexpensive, rapid and on-site monitoring such as fluorescence, diffuse reflectance and vibrational spectroscopy have been explored.[8] Among them, Raman spectroscopy has the potential to generate data with detailed molecular information. In addition, Raman spectroscopy is preferred for analysing bio-fluids and *in vivo* measurements as water is a weak Raman scatter due to the polar nature of the OH bond, providing minimum interference in the fingerprint region (200–1800 cm^{-1}).[9,10] Raman spectroscopy is generally a non-invasive approach used to gain chemical and structural information as well as to study molecular interactions.[11–13] It can be used for quantitative and qualitative analysis of a wide range of samples and materials. It has proven particularly useful in industrial and medical applications having resolved limitations of other spectroscopic techniques.[14] In biomedical optics and clinical applications, Raman spectroscopy in combination with multivariate analysis has proven its potential. The ability of detecting biochemical changes in tissues and cells can lead to a real time clinical diagnostic capabilities. Several studies have highlighted the importance of Raman spectroscopy for tissue differentiation in *ex vivo* and *in vivo* analysis.[15–17] Typically, a modern Raman spectrometer consist of an excitation source – usually a monochromatic laser, optical components to both transmit laser energy to specimen and collect back scattered signal, a notch filter to reject Rayleigh scattered light, a grating spectrometer and a high-end charged coupled device (CCD) camera to capture a Raman spectrum.

[a]*Tyndall National Institute, University College Cork, Cork, Ireland.*
E-mail: siddra.maryam@tyndall.ie
[b]*Cork University Dental School and Hospital, Wilton, Cork, Ireland*
[c]*XLIM Research Institute, UMR 7252 CNRS/Limoges University, Limoges, France*
[d]*ENTO Research Institute, University College Cork, Cork, Ireland*
[e]*South Infirmary Victoria University Hospital, Cork, Ireland*

This journal is © The Royal Society of Chemistry 2023

Open Access Article. Published on 06 March 2023. Downloaded on 7/20/2024 1:21:36 AM.
This article is licensed under a Creative Commons Attribution-NonCommercial 3.0 Unported Licence.

When the light from a laser interacts with the specimen, a small part of the incident energy is scattered inelastically (1 out of 10^6 photons) to produce a Raman spectrum.[18] In cases where the sample volume is too small or a microscopic area on a large sample needs to be analysed, a Raman spectrometry system coupled with a specially designed microscope would be desirable. Such instruments are commercially available at high cost and are bulky, non-portable, sample volume limited and are not considered suitable for point-of-care application. Additionally, Raman spectrometer coupled with the microscope are generally used as benchtop systems for *ex vivo* analysis owing to its bulkiness and limited flexibility to be used with the fibre optical probe and are therefore not suitable for clinical environment. To facilitate early detection at the primary-care level, as well as in research studies, we envision the use of a highly configurable spectrometry system suitable for seamless integration with the clinical procedure. Here, we describe an affordable, Raman-based instrument capable of both *in vivo* and *ex vivo* analysis employing single platform which can be easily wheeled to provide on-site testing and can be operated by a qualified clinician/lab technician with training and practice. Spectroscopic cell and supernatant analysis would be done to guide if biopsy sampling is necessary. After a positive test result of saliva or cell pellet analysis, *in vivo* measurements can be conducted just before tissue biopsy to guide for a suitable location of biopsy sampling and thereby provide improved sensitivity/specificity of diagnosis. Initially, the data analysis will be done by the experts, to later be automated after collecting sufficient data for machine learning models. To the best of our knowledge, this is the first report describing the design of multi-configurational Raman system addressing the limitations of the commercial clinical instruments.

The novel Raman system described here is compact, cost effective, portable and easy to assemble and align. It can easily fit into a console for transportation, thereby potentially facilitating point-of-care diagnostics. The design of our instrument is modular, consisting of the following:

Mode (A) Raman microscope – for *ex vivo* saliva cell pellet analysis.

Mode (B) Raman transmission stage – for saliva supernatant analysis using photonic crystal fibre (PCF).

Mode (C) Raman optical fibre probe – for *in vivo* tissue analysis.

This makes it suitable for both *in vivo* and *ex vivo* analysis and can be used in upright and transmission modes for liquid samples. The detailed optical design is given in the Methods section, enabling the easy adaptation by researchers in the field. In this study, we demonstrate the utility of our system in the context of oral cancer screening. The described system is only a prototype. Final system can employ centrifugation microfluidics[19] to separate cell pellet from supernatant, which will minimize human interventions. A typical work-flow of the procedure is shown in Fig. 1.

2. Experimental method

2.1 Instrumentation

Fig. 2 presents the configuration modes of the point-of-care Raman setup developed. This modular instrument consisted of: an illumination source, the sample probing subunit and

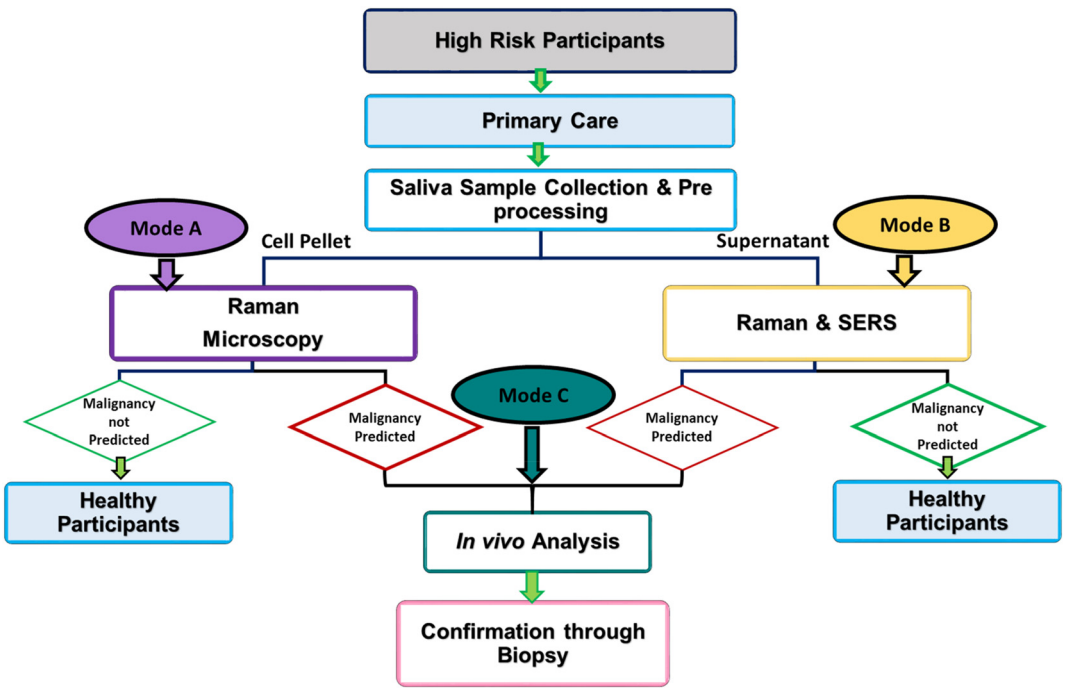

Fig. 1 Flow chart of study protocol with multi-configurational customised Raman system.

Open Access Article. Published on 06 March 2023. Downloaded on 7/20/2024 1:21:36 AM.
This article is licensed under a Creative Commons Attribution-NonCommercial 3.0 Unported Licence.

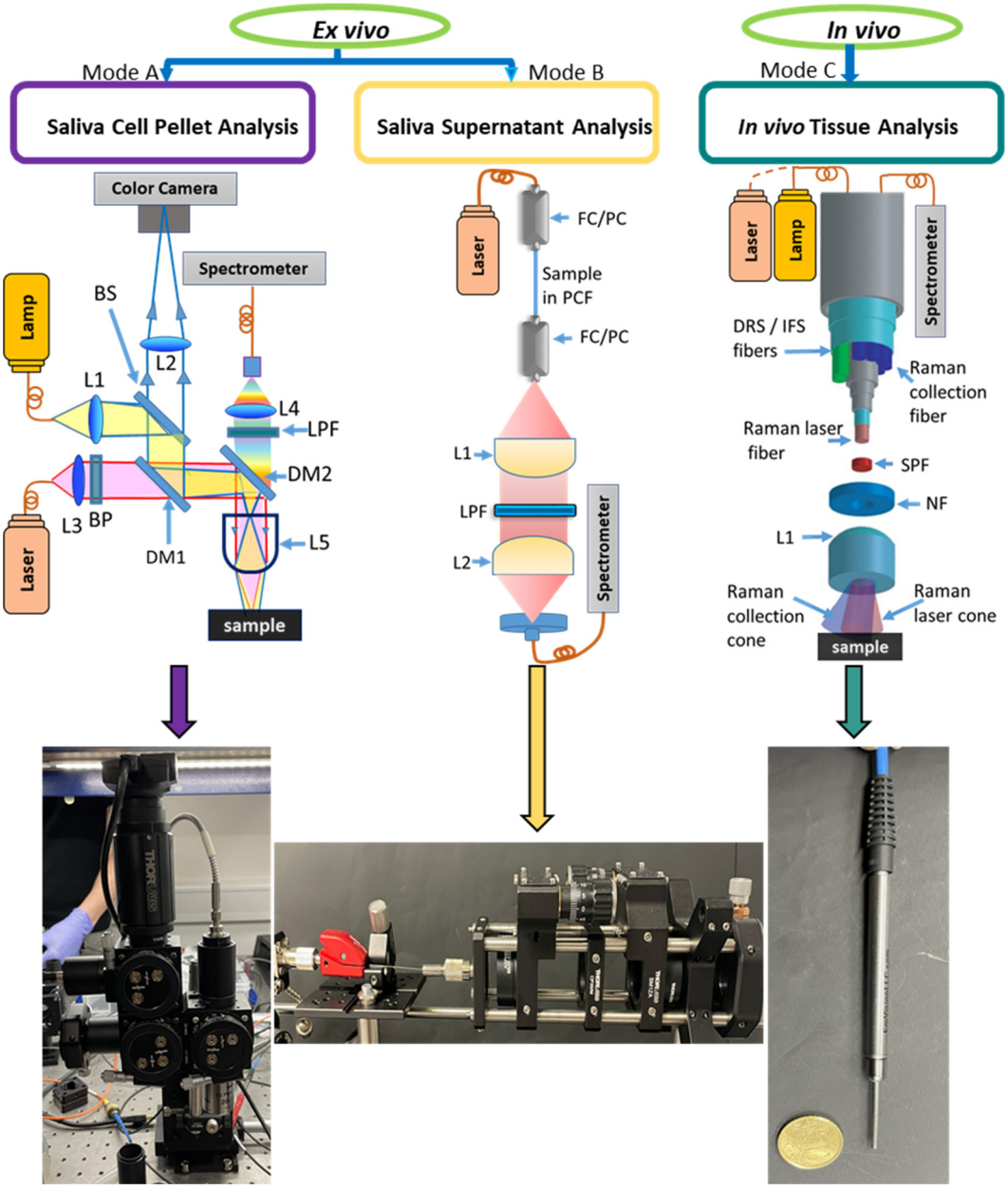

Fig. 2 Three configuration modes of the new customised Raman setup designed to include 3 plug and play modules to be coupled with common light sources and a spectrometer. These modes consist of: Mode (A) customised upright Raman microscope in combination with optical microscopy; Mode (B) transmission mode Raman stage; Mode (C) optical fibre probe for *in vivo* Raman analysis.

the spectrometer. Using the fibre optical connection between the subunits, the sample probing unit was easily switched between the three configuration modes. The illumination was achieved by a 785 nm narrow line width laser with high suppression of side bands (>60 dB suppression at 0.3 nm from the laser peak, Cobolt 08-01 Series, Cobolt, Sweden). The Raman spectrometer was equipped with a diffraction grating with 1200 groves per mm grating density (LS-785, Teledyne Princeton Instruments, USA), a 1340 × 400 pixels back illuminated CCD camera (Blaze: 400HR, Teledyne Princeton Instruments, USA). These subunits can be connected to the custom-built microscope (Fig. 2, Mode A). This is achieved fibre-optically using a round-to-linear bundle of a 7 × 200 μm core, (Thorlabs BFL200LS02). This Raman system can also utilise the customised transmission stage for the analysis of liquid specimens in transmission mode (Fig. 2, Mode B) and an optical fibre probe for the *in vivo* analysis (Fig. 2, Mode C). Currently, it takes up to five minutes to switch between configurations, mainly fibers. The light sources and calibration are the same for all three configurations. However, the final system will be more automated, which will seamlessly switch between different configurations. This prototype including

 This journal is © The Royal Society of Chemistry 2023

Open Access Article. Published on 06 March 2023. Downloaded on 7/20/2024 1:21:36 AM.
This article is licensed under a Creative Commons Attribution-NonCommercial 3.0 Unported Licence.

microscope and transmission mode stage is designed using off the shelf component in around 10k excluding the spectrometer and detector. The following section describes each of these configurations in detail with the novel optical design.

2.2 Mode (A) Raman microscope for *ex vivo* cell pellet analysis

Fig. 2, Mode A represents the customised Raman microscope which consists of a laser and a visible light source (for sample visualization) connected through optical fibres. Fibre coupled illumination allowed modification of the spot size on the sample plane. Further, this fibre guided light delivery makes the switching of different excitation wavelengths easy. Another important feature of this system is a flexible stage design, which can accommodate different specimen in different dimensions from mm to tens of cm. The specimen was illuminated through an objective lens and Raman scattered photons were collected *via* the same objective lens in backscattering mode and in turn, directed to the spectrometer *via* 7× round-to-linear low OH fibre bundle with 200 μm core (Thorlabs BFL200LS02). Simultaneously, a portion light from sample was patched to a CCD detector. This configuration was used for *ex vivo* analysis of solid and liquid specimens in the reflective mode.

White light imaging optical path. A broadband visible light source (Thorlabs M365LP1, 365 nm, 1350 mW mounted LED) was used to illuminate the specimen for conventional optical microscopy. The light beam entered the microscope *via* lens L1 (Thorlabs LA1951A, f = 25 mm) and redirected to the objective lens using a beam splitter BS (Thorlabs, BSW26R, 50 : 50, 350–1100 nm), dichroic mirror DM1 (Semrock, FF757-Di01) and dichroic mirror DM2 (Semrock LPD02-785RU). The L1 was arranged to provide uniform Kohler illumination of white light on the sample plane. The white light scattered from the sample was reflected by DM2 to DM1 which redirected it to a colour camera through BS and a field lens L2 (Thorlabs LB1437-A, f = 150 mm). A high-resolution coloured CMOS camera (Thorlabs DCC1645C) was used to visualize the sample under white light illumination. The field of view (FOV) was controlled using a microscope objective lens L4 (116 × 92 μm for 50×, 290 × 230 μm for 20× and 1160 × 920 μm for 5×). The images were displayed on computer screen using the Thorcam software.

Raman optical path. Monochromatic light (785 nm laser) passed through the collimation lens L3 (Thorlabs A397TM-B, f = 11 mm, NA (numerical aperture) = 0.3) and laser cleaning bandpass filter BP (Semrock LD01-785/10-25). Afterwards, the collimated excitation beam passed through the DM1 and was reflected by DM2, which was focused on the sample plane by microscope objective. The spot size of the focused excitation beam was 60 μm with 20× objective lens (Fig. 4). The Raman scattered photons from the sample passed through the objective lens and the excitation light is filtered out using a dichroic mirror (DM2) and long pass filter LPF (Semrock LP02-785RU-25). The filtered Raman light (free of excitation light) was focused on to a low OH circular to linear fibre bundle (Thorlabs BFL200LS02) using a lens L4 (Thorlabs F810SMA-850, f = 36.2 mm). The linear side of fibre was attached to the entrance linear slit of the Raman spectrometer. The Raman spectrometer subunit contained a filter chamber with a long pass filter (Semrock LP02-785RU-25), a high throughput spectrometer (Teledyne Princeton Instruments Acton LS785, f/2), and a highly sensitive deep depleted CCD camera (Blaze: 400HR, Teledyne Princeton Instruments, USA). The CCD pixels were binned vertically to combine light from linear slit. The light from the CCD is acquired using the LightField software (Teledyne Princeton Instruments, USA).

2.3 Mode (B) Raman transmission stage for saliva supernatant analysis using PCF

Fig. 2, Mode B and Fig. 3B illustrate a horizontal stage for liquid specimen analysis in transmission mode using PCF. PCF are optical fibers composed of periodic array of air-holes surrounding a solid or hollow-core. In this study, the fiber used is the simplest PCF that is composed of silica core (SC-PCF) at the intersection of three large air holes. Light is guided in the triangular core shape by the total internal reflection mechanism based on the large refractive index difference between the silica and air, and by the reduction of the thickness of the three silica struts enhancing light confinement in the core.[20,21] To integrate the inherently weak Raman signal from a liquid specimen (saliva supernatant) over a large volume, the SC-PCF with 3.5 μm core diameter, >70 μm air-channel diameter, and NA = 0.5 was filled with aqueous liquid. The external diameter (200 μm) of this SC-PCF is slightly larger than a standard fiber for allowing easier handling. In this SC-PCF, Raman signals are generated by the evanescent wave extended into the holes while excitation light (785 nm) propagates through the solid core.[20,22,23] The sample holder was used in this way to prolong light–sample interaction length, thereby improving detection sensitivity.[24] Another advantage with a longer path length than in a microscope was that the larger volume sampled can be more representative, especially for low concentration analytes. A further advantage was that still a very small volume of analyte was required (about 20–100 nl). A PCF filled with sample solution can be directly placed under the Raman microscope to collect the signal in conventional reflective mode. However, to ease the alignment of input laser beam in to the PCF, we designed a horizontal optical stage enabling the collection of signals in transmission mode. A 785 nm laser beam entered the PCF through an FC/PC connector (ferrule connector/physical contact connector). Raman signal emitted from the other end was collimated by an aspheric lens L1 (Thorlabs S-LAH64, f = 20 mm, NA = 0.54, ARC: 650–1050 nm). This lens was selected to match the NA of the PCF enhancing the collection efficiency. The collimated Raman signal, after passing through a long pass filter (LPF) (Semrock LP02-785RU-25), was collected by another lens L2 (Thorlabs N-BK7, f = 50 mm, NA = 0.23, ARC: 650–1050 nm) and focused on a low OH circular to linear fibre bundle (Thorlabs BFL200LS02). To transfer the

Open Access Article. Published on 06 March 2023. Downloaded on 7/20/2024 1:21:36 AM.
This article is licensed under a Creative Commons Attribution-NonCommercial 3.0 Unported Licence.

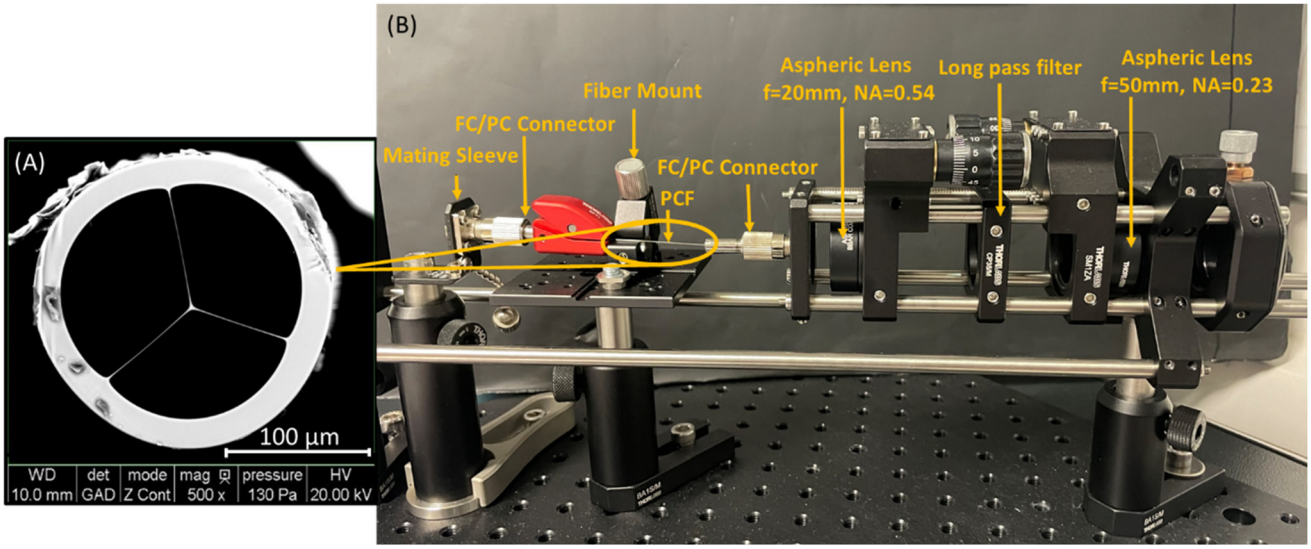

Fig. 3 (A) Cross section of a suspended core PCF designed by the authors (B) transmission mode stage for the analysis of liquid specimen injected into a PCF.

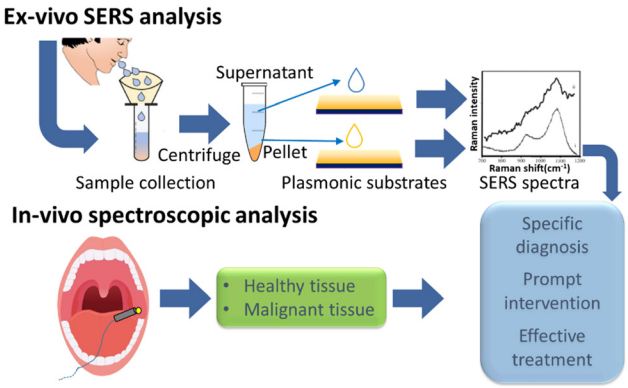

Fig. 4 Sample preparation and methodology for *ex vivo* saliva and *in vivo* tissue analysis.

signal to the spectrometer. The Fig. 3(A) shows the cross section of a typical suspended core PCF used in this study.

2.4 Mode (C) Raman optical fibre probe for *in vivo* tissue analysis

Fiber optics-based Raman spectroscopic system has a tremendous potential for real time *in vivo* tissue analysis in endoscopy or surgical guidance. However, for such applications small and flexible fiber optics probes are mandatory. This requirement has limited the clinical implementation of fiber optics based Raman technology for many years.[25] Recent advancement in fiber optics technology and miniaturization of the optical components have improved the *in vivo* implementation.[26–28] Fig. 2, Mode C shows a multi-spectroscopy fibre-optic probe (EMVision, Loxahatchee, FL, USA) used for the *in vivo* tissue analysis. This customised *in vivo* probe can be used to acquire spectra from multimodal spectroscopic techniques including Raman, fluorescence (FS) and diffuse reflectance spectroscopy (DRS). The probe consisted of 9 × 300 µm core diameter, 0.22 NA low OH silica fibres arranged in a concentric ring around a 300 µm core diameter, 0.22 NA low OH silica fibre used for Raman excitation. Seven out of nine fibres from the circular geometry collected the Raman signal passed through a donut shaped notch filter (NF), which rejected the laser line while transmitting the Raman signals from the probed tissue. The remaining two fibres can be used for DRS and FS. There was a short pass emission filter (SPF) in front of the central Raman illumination fibre to clean input laser line. A two-component customised lens L1 is placed at the probe tip to overlap the focus of excitations light and the area of collection of the Raman light from the tissue. Seven Raman collection fibres were aligned into a single line on the other end of the probe to deliver collected signals to the spectrometer *via* 50 µm slit. The accumulated signals from the seven fibres provide an optimum signal-to-noise ratio, needed for biological samples.

2.5 Sample preparation

Patients suffering from oral squamous cell carcinoma and other malignant diseases in the oral cavity going through biopsy and histopathological examination were enrolled in a study approved by the Clinical Research Ethics Committee (CREC) of University College Cork (CREC ref.: ECM 4 (y) 13/4/2021 & ECM 3 (cc) 11/05/2021). Written informed consent was obtained from human participants and study was performed in accordance with the Guidelines of Helsinki.

The performance of the multi-configuration Raman system was demonstrated for different healthy tissues of a single participant and using saliva sample collected from the same participant. A saliva specimen was collected and centrifuged at 10 000 rpm for 10 min at room temperature to separate it in supernatant and cell pellet and stored at −80 °C for further

 This journal is © The Royal Society of Chemistry 2023

Open Access Article. Published on 06 March 2023. Downloaded on 7/20/2024 1:21:36 AM.
This article is licensed under a Creative Commons Attribution-NonCommercial 3.0 Unported Licence.

use. For saliva sample analysis with the microscope, 3 drops of 10 μL saliva was placed and dried on a piece of aluminium foil. The cheek and red blood cells from the cell pellet were smeared on the aluminium foil to collect Raman spectra from a single cell layer.

To prepare the PCF sample for saliva analysis in transmission mode stage, a 9–10 cm long PCF with 3.5 μm core diameter and NA = 0.5 was cleaved at both ends. Its polymer jacket was removed from the ends and it was filled with saliva supernatant through capillary action.

In vivo analysis involves measurements on healthy tissues and lesion from the same participants using the fibre-optic probe. For the collection of *in vivo* Raman spectra, the probe was placed to just touch the area of interest.

2.6 Data analysis

Raman spectra were background corrected using the asymmetric least squares method,[29] noise smoothing with a Savitzky–Golay filter of polynomial order 2 and a window width of 7, and normalized to their respective mean intensity using MATLAB R2020b software (Mathworks, Inc., Natick, MA, USA).

3. Results and discussion

3.1 Mode (A) Raman microscope for *ex vivo* cell pellet analysis

Analysis of liquid biopsies has recently attracted attention as an emerging field in medical diagnosis. Biological fluids such as blood, saliva, urine and tears are rich in biomarkers that could be indicative of the health status of the sampled individual.[30–32] This provides a minimal invasive route for cancer screening and to classify cancer patients based on biomarkers identified.[33,34] The proposed Raman microscope can be used for the *ex vivo* analysis of any excised tissue or for liquid biopsies.

Fig. 5(A) illustrates Raman spectra from saliva specimen in both dried and liquid phase as well as from the mono layer of red blood cell and cheek cells as shown in Fig. 5B and C respectively. As can be seen, the Raman spectrum of saliva sample is featureless when wet but exhibits distinct peaks when dried. Several peaks characteristic of saliva are discernible.[35] For instance, peaks around 1049–1053 cm^{-1} are assignable to C–C stretching vibration of lipids. Furthermore, a well-known Raman bands characteristic of amide-I vibration of salivary proteins at around 1639–1670 cm^{-1} are also discernible. Also, unique to the saliva specimen are two additional peaks at 877 cm^{-1} and 938 cm^{-1} corresponding to a mixture of –C–O–C– and –C–C–, ring and stretching modes.[36] The Raman spectrum of red blood cell, on the other hand, was dominated by the haemoglobin signatures clearly differentiating it from cheek cell and saliva. Specifically, prominent peaks at around 1618 cm^{-1} and 1562 cm^{-1} can be assigned to the $C_a{=}C_b$ vibration of the vinyl groups, and C_β–C_β stretching modes in heme, respectively. Whereas peaks at 752 and 1395 are associated with pyrrole ring in heme. All the important differentiating Raman bands are presented in Table 1. Previously, Raman has been used to detect structural and biochemical changes in salivary analytes (*e.g.* proteins, amino acids, nucleic acids) accompanied with diseased transformation.[17] However due to generally weak signals and the strong background interference, most of the studies have been done on dried saliva samples to concentrate the analytes or utilized plasmon

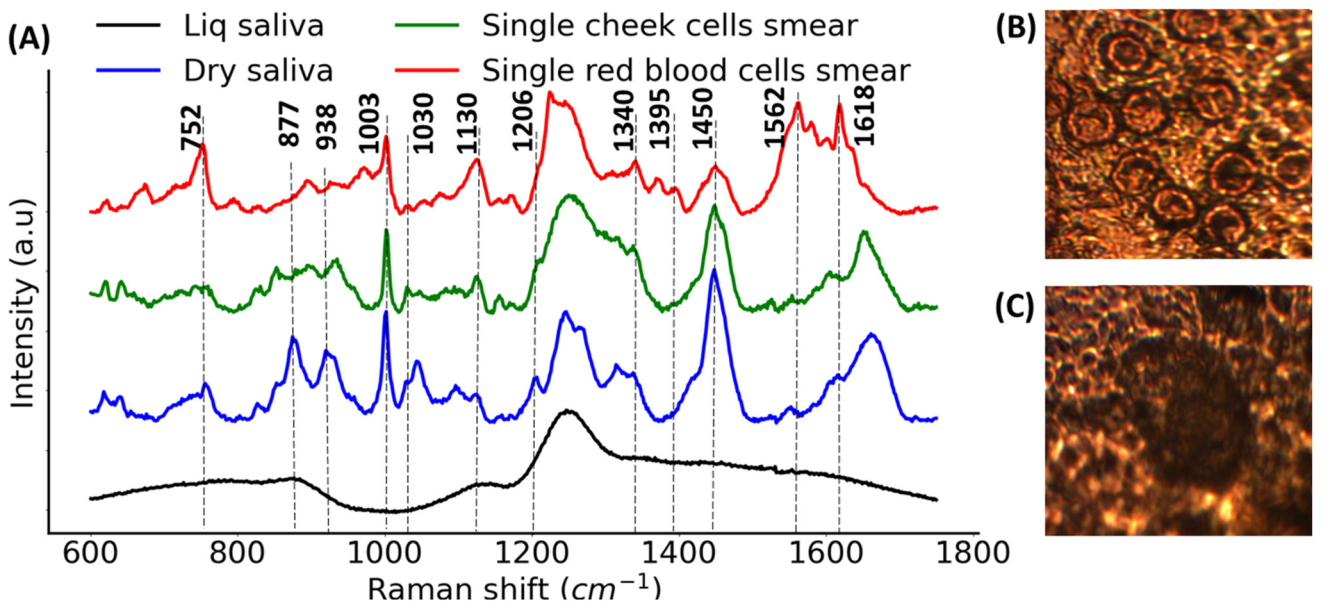

Fig. 5 (A) Pre-processed Raman spectra from saliva specimen in liquid and dry form. Right-optical microscopic view of (B) red blood cells (C) smeared cheek cell on aluminium foil.

Open Access Article. Published on 06 March 2023. Downloaded on 7/20/2024 1:21:36 AM. This article is licensed under a Creative Commons Attribution-NonCommercial 3.0 Unported Licence.

Table 1 Spectral assignment of the dominated Raman signatures observed in experimental data[36,40]

Wavenumber (cm^{-1})	Spectral assignments
752	ν(pyrrole breathing) stretch in heme; symmetric ring breathing in tryptophan
877	C–O–C ring (polysaccharides);C–C stretching (hydroxyproline)
938	C–O–C stretching (polysaccharides); C–C stretch α-helix proteins
960	PO_4^{3-} symmetric stretch (hydroxyapatite)
1003	Symmetric ring breathing mode of phenylalanine
1030	C–H in plane bending of phenylalanine
1080–1090	C–C stretch acyl chains (*gauche*) lipids; PO_2^- stretching (DNA); $\nu(C_\beta C_1)$ asymmetric stretch (hemoglobin)
1130	C–C stretch acyl chains (*trans*) lipids; C–O stretch polysaccharides; ν(pyrrole half-ring) asymmetric stretch (hemoglobin)
1204–1209	C–C_6H_5 stretch phenylalanine and tryptophan
1220–1320	Amide III-combination of NH in-plane bending and CN stretching
1302	CH_2 deformation (lipids)
1340	Nucleic acid (adenine, guanine); CH deformation polysaccharides
1395	ν(pyrrole quarter-ring) stretch (hemoglobin)
1440	CH_2 bending mainly in lipids
1450	CH_2 bending mainly in proteins
1562	$\nu(C_\beta C_\beta)$ stretch (hemoglobin)
1618	$\nu(C_a{=}C_b)$ of vinyl groups (hemoglobin)
1656	C=C stretch mainly in lipids
1630–1690	Amide I: mainly C=O stretch in proteins
1740	C=O in lipids

enhancement to improve the weak Raman signals from low concentration analytes.[37] The drying process leads to the structural/conformational changes of the analytes (*e.g.* proteins) and SERS struggles with reproducibility. The use of low NA longer focal depth objective lens (*e.g.* 5× or 10×) have poor collection efficiency and a focal length of tens of micron implies interaction of laser light with the sample is limited and thus requires long integration time, typically tens of seconds. These are not suitable for fast detection. Recently, fiber-enhanced Raman spectroscopy (FERS) where hollow core fibers and PCF have been used to confine the excitation light along the fiber (mm) length, thereby enabling the strong and efficient process of light–matter interactions (>50 times of conventional microscopic measurements) leading to enhanced Raman signals.[38,39] The sample volume probed at the focus of an objective will always be much smaller than the total volume probed over the length of these fibers.[38] To implement FERS, we developed the novel transmission mode stage (B) in which signal gets integrated over an extended interaction length with the light.[23,38,39]

3.2 Mode (B) Raman transmission stage for saliva supernatant analysis using PCF

The interaction of light with the analytes along the PCF length is critical for sensitive detection of low concentration analytes. In such measurements one must consider light attenuation yielding a reduction of transmission signal due to scattering and absorption. It is thus important to characterize the optimum PCF length. For this, the transmission stage was used to optimize the length of PCF using vegetable oil as an analyte because its consistency and refractive index is close to that of saliva (for saliva refractive index $n \approx 1.4$ and for oil $n \approx 1.46$).[41,42] It also has a distinct Raman signal as discussed in Table 1. Different lengths of PCF ranging from 9 cm to 13 cm were tested. The results are shown in Fig. 6A, highlighting the maximum Raman signal for 9 cm and 10 cm PCF lengths. Subsequent increase in the length >10 cm of the PCF lead to gradual decrease in Raman photons due to absorption/scattering loss. The curves in the Fig. 6B represent Raman signals for different modes of our new Raman system using oil as an

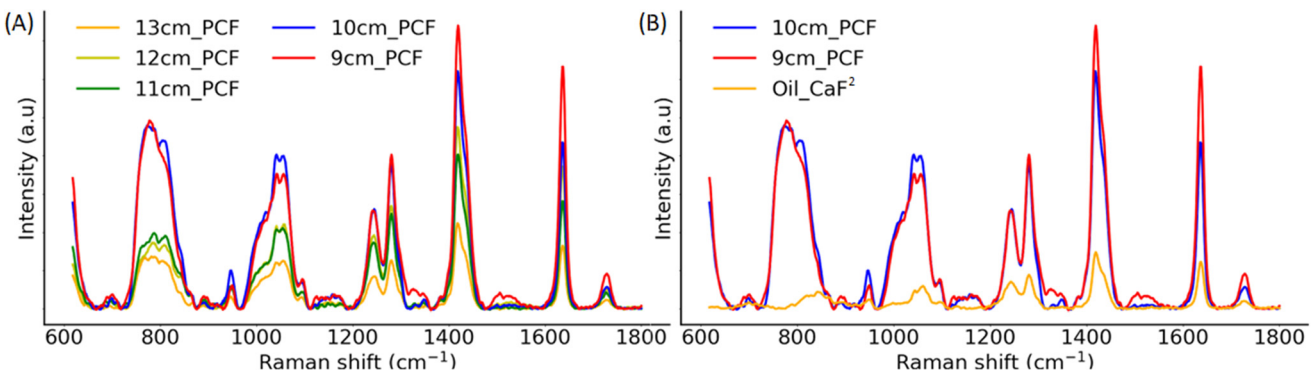

Fig. 6 Comparison of Raman spectra from (A) different length of PCF using vegetable oil as an analyte (B) different instrument configuration modes of the customized system using oil as analyte.

This journal is © The Royal Society of Chemistry 2023

Open Access Article. Published on 06 March 2023. Downloaded on 7/20/2024 1:21:36 AM.
This article is licensed under a Creative Commons Attribution-NonCommercial 3.0 Unported Licence.

analyte. 9 cm and 10 cm PCF filled with oil provided the highest signals when analysed using transmission mode as compared the oil placed on a 2D CaF_2 substrate and analysed with Microscope in reflection mode. This improvement of signals in PCF compared to 2D substrates would be critical in detecting low concentration oral cancer markers in saliva.

The spectra in Fig. 7 represents Raman signals of 50 μM solution of Rhodamine B (Rhd B) in water filled in the PCF and observed in transmission mode *vs.* on a CaF_2 substrate and observed under the microscope in reflection mode. Rhd B peaks that were difficult to see on a 2D CaF_2 substrate under the microscope were significantly stronger when analysed through PCF due to increased interaction between the excitation laser and analyte over the length of 9 cm. The observed Rhd B peaks were in line with the previously published literature.[43]

3.3 Mode (C) Raman optical fibre probe for *in vivo* tissue analysis

Over the time, Raman spectra of various tissue has been observed. Most recognized Raman scatterers are blood, lipid, collagen, tyrosine elastin, myoglobin, carotenoids and nucleic acids *etc*.[17,44,45] Fig. 8 represents spectra from different tissue types in the oral cavity collected from a healthy participant with the customised fibre optic probe. The probe was gently placed on the area of interest to collect the Raman data from various tissues. 30 mW laser power was used to collect signal for a time of 4 s, to keep the energy per unit area within the permissible limit of the tissue.

The difference between different tissue types was clearly visible, especially signal from mandible bone was quite prominent at 960 cm^{-1} in the data collected from human gingiva while the lip Raman spectrum was dominated by lipid signals at 1080, 1302, 1440 and 1740 cm^{-1}.[46,47] Other subtle differences in these three different tissue types can be seen in terms of peak height and width at 1003 and 1660 cm^{-1} respectively. The molecular vibrational modes associated with these changes are tabulated in Table 1.

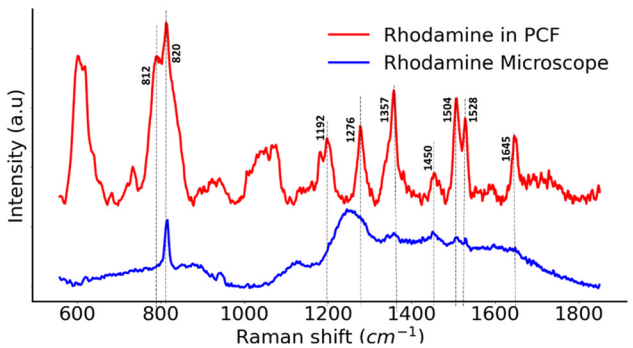

Fig. 7 Raman spectra comparison of Rhd B-filled in the PCF *vs.* on a 2 dimensional CaF_2 substrate.

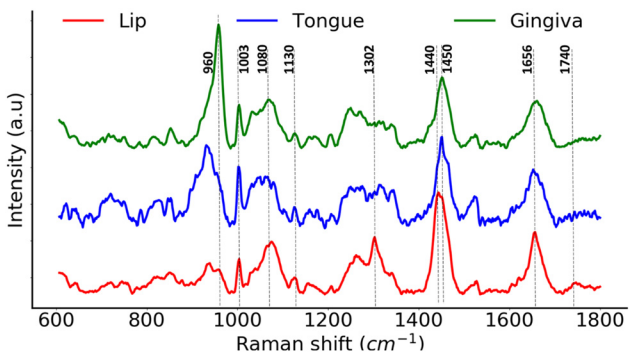

Fig. 8 Spectra from different tissue types in oral cavity collected from the new customised Raman system.

4. Conclusion

Design development and assembly of a versatile customised Raman system is reported in this study. This system can work in three different modes. The first mode was Raman microscope combined with conventional optical microscopy. This microscope has a flexible stage design for sample of different dimensions. We also demonstrated the benefit of the custom built liquid sample transmission stage over microscope in collecting signals from low concentration analytes. This PCF based transmission set-up enabled stronger Raman signals in a relatively small volume. Lastly, the flexible optical fibre based probe is suitable to acquire multiple (Raman, diffuse reflectance and fluorescence) spectroscopic techniques data from the same tissue location *in vivo*. In summary, this flexible Raman system is of great potential for the early diagnosis of oral cancer *via* initial screening using participants saliva followed by Raman spectral signatures guided biopsy of the lesions. The flexible and modular design can be of interest to Raman spectroscopy community and potentially in future primary care.

Author contributions

Siddra Maryam: methodology, system design and development, experiments, data analysis, writing, review and editing; Sanathana Konugolu Venkata Sekar: system design and development, review and editing; Daniyal Ghauri: data collection; Edward Fahy: data acquisition, recruiting participant, manuscript review; Marcelo Saito Nogueira: project planning, manuscript review; Huihui Lu: project planning, manuscript review; Flavien Beffara: PCF design and fabrication; Georges Humbert: PCF design and fabrication; Richeal Ni Riordain: supervision and managing clinical collaboration; Patrick Sheahan: supervision; Ray Burke: supervision and managing clinical collaboration; Kiang Wei Kho: system design and development, experiments, review and editing; Rekha Gautam: system design and development, experiment, data analysis, writing, review and editing; Stefan Andersson-Engels: funding, conceptualization, supervision, review and editing.

Open Access Article. Published on 06 March 2023. Downloaded on 7/20/2024 1:21:36 AM.
This article is licensed under a Creative Commons Attribution-NonCommercial 3.0 Unported Licence.

Conflicts of interest

There are no conflicts to declare.

Acknowledgements

We greatly acknowledge fruitful discussions with Dr Linda Feeley. The authors will also like to thanks Jean Matias for his help in laser beam profile characterization and to Konstantin Grygoryev for his proof reading and improving the English in the manuscript. The authors are grateful for the financial support of Science Foundation Ireland through contract SFI/15/RP/2828.

References

1 P. Speight and P. Farthing, The pathology of oral cancer, *Br. Dent. J.*, 2018, **225**(9), 841–847.
2 D. Conway, M. Purkayastha and I. Chestnutt, The changing epidemiology of oral cancer: definitions, trends, and risk factors, *Br. Dent. J.*, 2018, **225**(9), 867–873.
3 C. N. E. Board, Oral and Oropharyngeal Cancer: Statistics, **https://www.cancer.net/cancer-types/oral-and-oropharyngeal-cancer/statistics#:~:text=The%20overall%205%2Dyear%20survival,HPV%20(see%20Risk%20Factors)**.
4 L. P. Kowalski, R. Bagietto, J. R. Lara, R. L. Santos, J. F. Silva Jr. and J. Magrin, Prognostic significance of the distribution of neck node metastasis from oral carcinoma, *Head Neck*, 2000, **22**(3), 207–214.
5 F. P. Koch, M. Kunkel, S. Biesterfeld and W. Wagner, Diagnostic efficiency of differentiating small cancerous and precancerous lesions using mucosal brush smears of the oral cavity—a prospective and blinded study, *Clin. Oral Investig.*, 2011, **15**(5), 763–769.
6 H. J. Byrne, I. Behl, G. Calado, O. Ibrahim, M. Toner, S. Galvin, C. M. Healy, S. Flint and F. M. Lyng, Biomedical applications of vibrational spectroscopy: Oral cancer diagnostics, *Spectrochim. Acta, Part A*, 2021, **252**, 119470.
7 M. H. Al-Azri, Delay in cancer diagnosis: causes and possible solutions, *Oman Med. J.*, 2016, **31**(5), 325.
8 L. Marcu, Fluorescence lifetime techniques in medical applications, *Ann. Biomed. Eng.*, 2012, **40**(2), 304–331.
9 G. Calado, I. Behl, A. Daniel, H. J. Byrne and F. M. Lyng, Raman spectroscopic analysis of saliva for the diagnosis of oral cancer: A systematic review, *Transl. Biophotonics*, 2019, **1**(1–2), e201900001.
10 Z. Li, M. J. Deen, S. Kumar and P. R. Selvaganapathy, Raman spectroscopy for in-line water quality monitoring—Instrumentation and potential, *Sensors*, 2014, **14**(9), 17275–17303.
11 P. Vandenabeele, *Practical Raman spectroscopy: an introduction*, Wiley Online Library, 2013.
12 A. Orlando, F. Franceschini, C. Muscas, S. Pidkova, M. Bartoli, M. Rovere and A. Tagliaferro, A comprehensive review on Raman spectroscopy applications, *Chemosensors*, 2021, **9**(9), 262.
13 S. J. Owonubi, N. M. Malima and N. Revaprasadu, Metal oxide-based nanocomposites as antimicrobial and biomedical agents, *Antibiotic materials in healthcare*, Elsevier, 2020, pp. 287–323.
14 A. Synetos and D. Tousoulis, Invasive imaging techniques, *Coronary Artery Disease: From Biology to Clinical Practice*, 2017, p. 359.
15 J. Zhang, Y. Fan, Y. Song and J. Xu, Accuracy of Raman spectroscopy for differentiating skin cancer from normal tissue, *Medicine*, 2018, **97**(34), e12022.
16 G. Donjuán-Loredo, R. Espinosa-Tanguma, M. León-Bejarano, R. Salgado-Delgado, F. J. González, E. Guevara and M. Ramírez-Elías, Raman spectroscopy for adipose tissue differentiation: a pilot study, *Optical Tomography and Spectroscopy*, Optical Society of America, 2020, p. JW3A.12.
17 S. Maryam, M. S. Nogueira, R. Gautam, S. Krishnamoorthy, S. K. Venkata Sekar, K. W. Kho, H. Lu, R. Ni Riordain, L. Feeley, P. Sheahan, R. Burke and S. Andersson-Engels, Label-Free Optical Spectroscopy for Early Detection of Oral Cancer, *Diagnostics*, 2022, **12**(12), 2896.
18 D. C. Harris and M. D. Bertolucci, *Symmetry and Spectroscopy*, Dover Publications, Inc., New York, 1978.
19 U. Y. Schaff and G. J. Sommer, Whole blood immunoassay based on centrifugal bead sedimentation, *Clin. Chem.*, 2011, **57**(5), 753–761.
20 U. S. Dinish, F. Beffara, G. Humbert, J.-L. Auguste and M. Olivo, Surface-enhanced Raman scattering-active photonic crystal fiber probe: Towards next generation liquid biopsy sensor with ultra high sensitivity, *J. Biophotonics*, 2019, **12**(11), e201900027.
21 A. V. Markin, N. E. Markina and I. Y. Goryacheva, Raman spectroscopy based analysis inside photonic-crystal fibers, *TrAC, Trends Anal. Chem.*, 2017, **88**, 185–197.
22 Y. Zhang, C. Shi, C. Gu, L. Seballos and J. Z. Zhang, Liquid core photonic crystal fiber sensor based on surface enhanced Raman scattering, *Appl. Phys. Lett.*, 2007, **90**(19), 193504.
23 F. Beffara, J. Perumal, A. Puteri Mahyuddin, M. Choolani, S. A. Khan, J. L. Auguste, S. Vedraine, G. Humbert, U. Dinish and M. Olivo, Development of highly reliable SERS-active photonic crystal fiber probe and its application in the detection of ovarian cancer biomarker in cyst fluid, *J. Biophotonics*, 2020, **13**(3), e201960120.
24 F. Beffara, G. Humbert, J.-L. Auguste, J. Perumal, U. Dinish and M. Olivo, Optimization and performance analysis of SERS-active suspended core photonic crystal fibers, *Opt. Express*, 2020, **28**(16), 23609–23619.
25 L. F. Santos, R. Wolthuis, S. Koljenović, R. M. Almeida and G. J. Puppels, Fiber-optic probes for in vivo Raman spectroscopy in the high-wavenumber region, *Anal. Chem.*, 2005, **77**(20), 6747–6752.
26 A. K. Barik, J. Lukose, R. Upadhya, M. V. Pai, V. Kartha and S. Chidangil, In vivo spectroscopy: optical fiber probes for

This journal is © The Royal Society of Chemistry 2023

Open Access Article. Published on 06 March 2023. Downloaded on 7/20/2024 1:21:36 AM.
This article is licensed under a Creative Commons Attribution-NonCommercial 3.0 Unported Licence.

clinical applications, *Expert Rev. Med. Devices*, 2022, **19**(9), 657–675.

27 M. G. Shim, B. C. Wilson, E. Marple and M. Wach, Study of fiber-optic probes for in vivo medical Raman spectroscopy, *Appl. Spectrosc.*, 1999, **53**(6), 619–627.

28 M. Plesia, O. A. Stevens, G. R. Lloyd, C. A. Kendall, I. Coldicott, A. J. Kennerley, G. Miller, P. J. Shaw, R. J. Mead and J. C. Day, In vivo fiber optic Raman spectroscopy of muscle in preclinical models of amyotrophic lateral sclerosis and Duchenne muscular dystrophy, *ACS Chem. Neurosci.*, 2021, **12**(10), 1768–1776.

29 R. Gautam, D. Peoples, K. Jansen, M. O'Connor, G. Thomas, S. Vanga, I. J. Pence and A. Mahadevan-Jansen, Feature Selection and Rapid Characterization of Bloodstains on Different Substrates, *Appl. Spectrosc.*, 2020, **74**(10), 1238–1251.

30 R. Gautam, J. Y. Oh, R. P. Patel and R. A. Dluhy, Non-invasive analysis of stored red blood cells using diffuse resonance Raman spectroscopy, *Analyst*, 2018, **143**(24), 5950–5958.

31 J. M. Connolly, K. Davies, A. Kazakeviciute, A. M. Wheatley, P. Dockery, I. Keogh and M. Olivo, Non-invasive and label free detection of oral squamous cell carcinoma using saliva surface-enhanced Raman spectroscopy and multivariate analysis, *Nanomedicine*, 2016, **12**, 1593–1601.

32 S. Hu, J. A. Loo and D. T. Wong, Human body fluid proteome analysis, *Proteomics*, 2006, **6**(23), 6326–6353.

33 A. Alba-Bernal, R. Lavado-Valenzuela, M. E. Domínguez-Recio, B. Jiménez-Rodriguez, M. I. Queipo-Ortuño, E. Alba and I. Comino-Méndez, Challenges and achievements of liquid biopsy technologies employed in early breast cancer, *EBioMedicine*, 2020, **62**, 103100.

34 S. Maryam, M. S. Nogueira, S. K. Moorthy, S. Sekar, H. Lu, R. Gautam, R. Burke, S. Andersson-Engels, R. N. Riordain and P. Sheahan, Multi-configuration Raman spectrometer for early stage diagnosis of oral cancer, *Biomedical Vibrational Spectroscopy 2022: Advances in Research and Industry*, SPIE, 2022, pp. 20–26.

35 H. J. Koster, A. Guillen-Perez, J. S. Gomez-Diaz, M. Navas-Moreno, A. C. Birkeland and R. P. Carney, Fused Raman spectroscopic analysis of blood and saliva delivers high accuracy for head and neck cancer diagnostics, *Sci. Rep.*, 2022, **12**(1), 18464.

36 Z. Movasaghi, S. Rehman and I. U. Rehman, Raman Spectroscopy of Biological Tissues, *Appl. Spectrosc. Rev.*, 2007, **42**(5), 493–541.

37 S. Feng, S. Huang, D. Lin, G. Chen, Y. Xu, Y. Li, Z. Huang, J. Pan, R. Chen and H. Zeng, Surface-enhanced Raman spectroscopy of saliva proteins for the noninvasive differentiation of benign and malignant breast tumors, *Int. J. Nanomed.*, 2015, **10**, 537.

38 H. Ding, D. J. J. Hu, X. Yu, X. Liu, Y. Zhu and G. Wang, Review on All-Fiber Online Raman Sensor with Hollow Core Microstructured Optical Fiber, *Photonics*, 2022, 134.

39 B. G. Eleftheriades, E. E. Storey and A. S. Helmy, Label-Free Spontaneous Raman Sensing in Photonic Crystal Fibers with Nanomolar Sensitivity, *Adv. Opt. Mater.*, 2022, **10**(6), 2101117.

40 B. R. Wood, P. Caspers, G. J. Puppels, S. Pandiancherri and D. McNaughton, Resonance Raman spectroscopy of red blood cells using near-infrared laser excitation, *Anal. Bioanal. Chem.*, 2007, **387**(5), 1691–1703.

41 M. Cárdenas, T. Arnebrant, A. Rennie, G. Fragneto, R. K. Thomas and L. Lindh, Human saliva forms a complex film structure on alumina surfaces, *Biomacromolecules*, 2007, **8**(1), 65–69.

42 L. Coelho, D. Viegas, J. L. C. O. Santos and J. M. M. M. de Almeida, Monitoring of high refractive index edible oils using coated long period fiber grating sensors, *Optical Sensors 2015*, SPIE, 2015, pp. 248–254.

43 M. Liu, R. Xiang, Y. Lee, K. Otsuka, Y.-L. Ho, T. Inoue, S. Chiashi, J.-J. Delaunay and S. Maruyama, Fabrication, characterization, and high temperature surface enhanced Raman spectroscopic performance of SiO_2 coated silver particles, *Nanoscale*, 2018, **10**(12), 5449–5456.

44 J. Desroches, M. Jermyn, M. Pinto, F. Picot, M.-A. Tremblay, S. Obaid, E. Marple, K. Urmey, D. Trudel and G. Soulez, A new method using Raman spectroscopy for in vivo targeted brain cancer tissue biopsy, *Sci. Rep.*, 2018, **8**(1), 1792.

45 H. Zeng, J. Zhao, M. Short, D. I. Mclean, S. Lam, A. Mcwilliams and H. Lui, Raman spectroscopy for in vivo tissue analysis and diagnosis, from instrument development to clinical applications, *J. Innovative Opt. Health Sci.*, 2008, **1**(01), 95–106.

46 P. Meksiarun, B. B. Andriana, H. Matsuyoshi and H. Sato, Non-invasive quantitative analysis of specific fat accumulation in subcutaneous adipose tissues using Raman spectroscopy, *Sci. Rep.*, 2016, **6**(1), 1–8.

47 M. V. Schulmerich, J. H. Cole, K. A. Dooley, M. D. Morris, J. M. Kreider, S. A. Goldstein, S. Srinivasan and B. W. Pogue, Noninvasive Raman tomographic imaging of canine bone tissue, *J. Biomed. Opt.*, 2008, **13**(2), 020506.